*Environ. Sci. Technol.* **1998**, *32,* 3228−3236

# An Automated System for the Measurement of Nitrogen Oxides and Ozone Concentrations from a Passenger Aircraft: Instrumentation and First Results of the NOXAR Project

PETER DIAS-LALCACA,*,† DOMINIK BRUNNER,‡ WALTER IMFELD,† WERNER MOSER,† AND JOHANNES STAEHELIN‡

*ECO PHYSICS AG, P.O. Box 282, CH-8635 Dürnten, Switzerland, and Institute for Atmospheric Sciences, ETH-Hönggerberg, CH-8093 Zurich, Switzerland*

A fully automated system for measuring NO, $NO_2$, and $O_3$ in the upper troposphere and lower stratosphere from a passenger aircraft is described. Detection limits ($1\sigma$) of 23, 45, and 500 pptv were achieved for NO, $NO_2$, and $O_3$, respectively, for a 2 min integration time during flights. Continuous measurements were made during a 1 year period ending May 1996 on a total of 540 flights between Zurich and destinations in the United States and the Far East. The measurements represent about a 10-fold increase in the coverage of presently available $NO_x$ measurements in the tropopause region. The measurement hardware, based on commercially available instrumentation and specifically designed to meet the very stringent safety regulations normal in civil aviation, is described, and first results are briefly reported.

## Introduction

Nitrogen oxides ($NO_x = NO + NO_2$) are important precursors for the formation of ozone and other photooxidants in the troposphere (*1*). High ozone concentrations in ambient air can produce adverse effects on human health (*2*) and reduce crop yields (*3*). Furthermore, tropospheric ozone is a strong greenhouse gas, and recent numerical model results have revealed that the increase in tropospheric ozone has contributed significantly to global radiative forcing since the last century (*4*).

Emissions from current subsonic air traffic are an important source of $NO_x$ at cruise altitudes (8−12 km asl) close to the tropopause in midlatitudes where the greenhouse efficiency of $O_3$ is a maximum (*5*). The $O_3$ production rate depends strongly on the $NO_x$ concentration, and numerical model simulations indicate that the net ozone production rate under the conditions typical of the upper troposphere is highest at $NO_x$ concentrations of a few hundred pptv (*6*). An adequate knowledge of the distribution of $NO_x$ in the tropopause region is thus crucial for the assessment of the influence of present and future air traffic emissions on the atmosphere, which is currently the subject of intense investigation. Related research topics include air traffic exhaust emission of nitrogen oxides and ozone formation based on in situ measurements and model calculations (*7*−*11*). Various chemical transport models have been developed to address the problem of ozone concentrations in the upper troposphere and the possible effects of nitrogen oxide emissions (*6, 12*−*14*) from aircraft. However, other nitrogen oxide sources such as fossil fuel combustion, biomass burning, soil emission, and lightning also contribute to the upper tropospheric nitrogen oxide and ozone concentrations, and present knowledge about these emission sources and their influence on upper tropospheric $NO_x$ concentration is inadequate (*15*). Current chemical transport models have different strong points since they give varying weights to photochemical transformation schemes and atmospheric transport. The accuracy of these models must be evaluated by comparison with actual measurements of the key chemical species involved. However, only a limited number of measurements of nitrogen oxides in the free troposphere is presently available (*16*).

Measurements made from scientific aircraft are invaluable for studying important atmospheric chemical and physical processes in detail (*17*). However, such campaigns usually cover only a small part of the globe and involve measurements over a period of at most a few weeks and can therefore not provide a representative image of the distribution of short-lived and highly variable tracers such as $NO_x$. A complementary research approach is the use of commercial aircraft as measuring platforms, for example in the Global Atmospheric Sampling Program (GASP) in the late 1970s (*18*) and, more recently, in the Measurement of Ozone on Airbus In-Service Aircraft (MOZAIC) project (*19*).

In the NOXAR project (Nitrogen Oxides and Ozone along Air Routes), nitrogen oxides (NO and $NO_2$) and ozone concentrations were measured continuously over a 1 year period along selected air routes using a Swissair B-747 aircraft as the measuring platform. The low $NO_x$ concentrations expected at cruising altitude required highly sensitive analyzers with good temporal resolution. The latter characteristic is essential for good spatial resolution given the high speed of the aircraft (about 250 m/s) and the fact that nitrogen oxide and ozone concentrations can change rapidly, for example when the aircraft crosses the exhaust plume of another airplane or when steep ozone concentration gradients are encountered in the vicinity of the jet stream. Furthermore, the instrumentation system had to be robust enough to operate reliably under the severe conditions encountered in an aircraft freight compartment. In this paper, the instrumentation is described, and typical features of the $NO_x$ and ozone distribution observed during measurements are briefly discussed.

## Instrumentation

To achieve the desired goal of measuring nitrogen oxides and ozone at aircraft cruising altitudes (typically 10−12 km above sea level) with the greatest possible accuracy, reliability, and temporal resolution from the passenger aircraft platform, it was necessary during the system design phase to take into account the many, often conflicting, requirements imposed by instrumental, scientific, budgetary, flight-operational, and safety considerations. The most important criteria the system had to meet are in summary: (a) fully automated and totally transparent to flight operations, (b) stringent fire and mechanical safety requirements, (c) lowest possible weight and power consumption while not exceeding a given volume,

* Corresponding author phone: +41-55-240-4343; fax: +41-55-240-8585; e-mail: rd.ecophysics@active.ch.
† ECO PHYSICS AG.
‡ Institute for Atmospheric Sciences.


S0013-936X(98)00119-9 CCC: $15.00 
Published on Web 09/04/1998

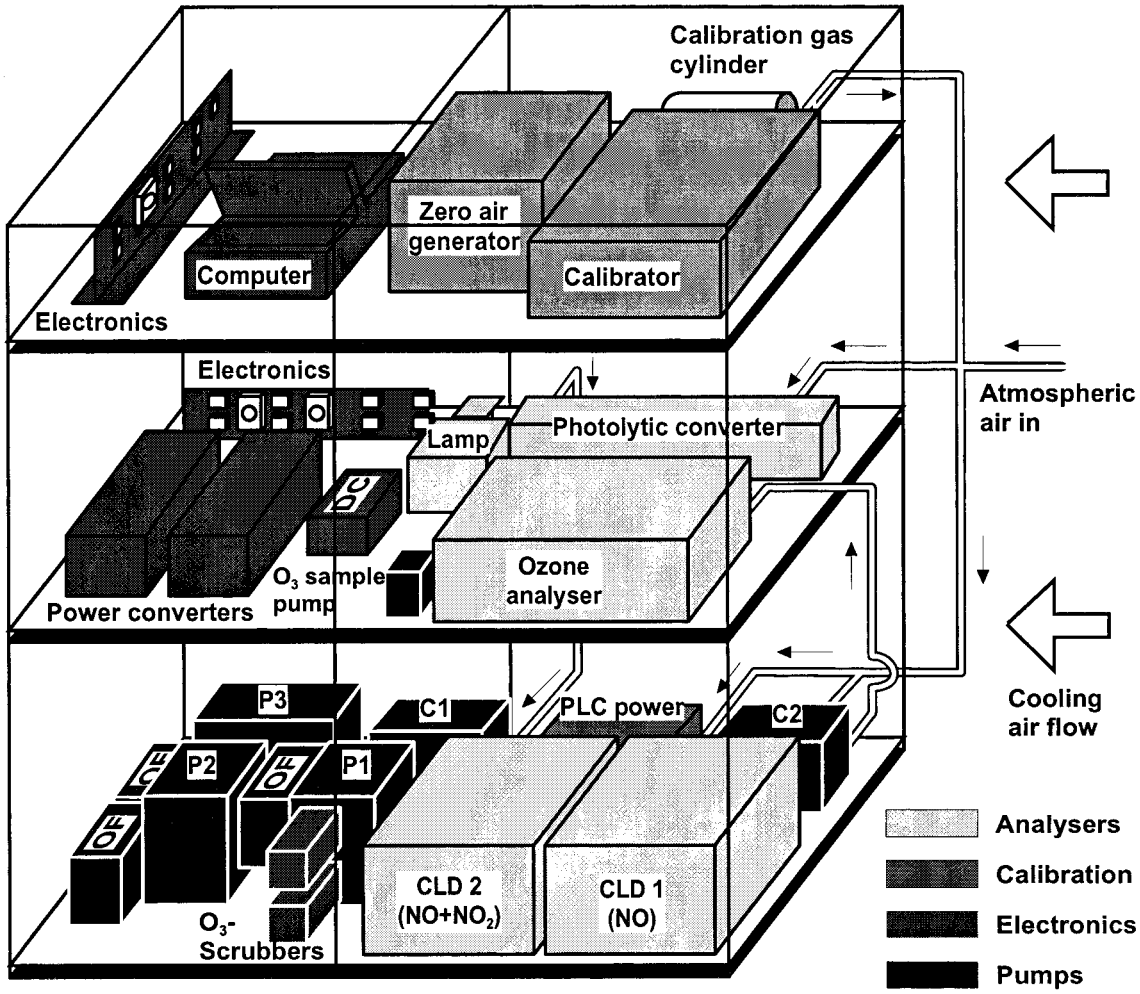


**FIGURE 1. Block diagram of main system components. The heaviest equipment is mounted on the bottom shelf to improve mechanical stability. The "clean" equipment (i.e., analyzers, calibrator, and zero air generator) is located in the right-hand side of the rack where the cooling air enters, whereas the "dirty" equipment (i.e., vacuum pumps, zero air compressor, power converters), which also has a generally higher operating temperature, is located in the left-hand compartment. Abbreviations: DC, DC power supply; P1, P2, P3, vacuum pumps for CLD1, CLD2, and the bypass system; C1, compressor for zero air generator; C2, compressor for ozone instrument sample; OF, oil mist filters for vacuum pumps (3×).**

(d) allow rapid installation and removal from the aircraft, (e) capable of tolerating the electrically and mechanically severe environment of an airliner freight compartment, and (f) permit rapid and easy internal access for data retrieval, maintenance, and repair.

To achieve these aims, the instrumentation package was designed to use existing commercially available NO, $NO_2$, and $O_3$ analyzers, modified where necessary and installed together with all the auxiliary equipment (vacuum pumps, power supplies, pure air generator, electronic circuitry, calibrator, control computer) in a purpose-built rack designed to meet the stringent safety requirements normal in civil aviation. A block diagram of the layout of the main instrumentation modules is shown in Figure 1, and the actual location of the rack in the aircraft is depicted in Figure 2.

**NO Analyzer.** A commercially available ECO PHYSICS CLD 780 TR analyzer (CLD1 in Figures 1 and 3) was used to measure nitric oxide concentrations. This instrument detects the chemiluminescent signal generated when NO-containing sample gas is mixed with an excess of internally generated ozone in a reaction chamber held at constant temperature and known pressure. The instrument's relatively high flow rate of 3 L/min (STP) and low internal pressure (inlet pressure, 85 hPa; reaction chamber pressure, 15 hPa) help ensure a 0−95% rise time of less than 1 s, where rise time means the time required after a stepwise increase in sample concentration for the instrument to achieve a reading of 95% of the final value. The mumetal-shielded photomultiplier tube (PMT) is cooled by a closed-cycle refrigerator unit to about −30 °C. It is operated in photon-counting mode, producing about 1000 counts/s per ppbv of NO with a zero signal (i.e., instrument background signal with no NO in the sampled gas) of about 1000 counts/s at ground level. The instrument performance would have been enhanced by almost a factor of 2 had the ozone generators been supplied with $O_2$, but this option was precluded on safety grounds, so dry air was used instead. The effect of chemical interference in the sample may be removed by using a prechamber during the zero signal measurement, which allows the completion of the fast $NO/O_3$ chemiluminescence reaction before the gas mixture reaches the main chamber, where the slower interferent reaction then provides a reliable baseline signal. This process removes interference effects due to hydrocarbons and minimizes $NO_y$ interference (*20*). However, since interferences from other species were expected to be negligible under the conditions in the tropopause region, the prechamber technique was not used during the NOXAR measurements.

Exhaust gas from the analyzer is drawn through a thermal ozone scrubber (ECO PHYSICS) and into the vacuum pump

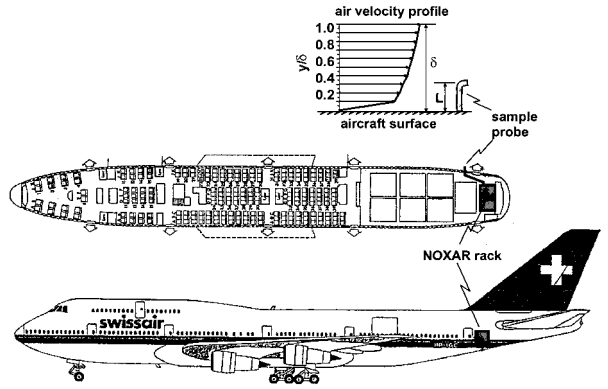


**FIGURE 2. The NOXAR rack is located and anchored like a cargo palette in the rearmost section of the upper cargo deck of a Swissair Boeing B-747-357 Combi aircraft. The top part of the figure shows a schematic of the rearward facing sample probe which extends $L = 9$ in. into the slipstream of the aircraft. The thickness $\delta$ of the boundary layer of the aircraft is about 27 in. at this point, thus encompassing the inlet. The mean air velocity profile in the boundary layer is shown schematically. At distance $y = L$ from the surface, the velocity is approximately 80% of the velocity of the undisturbed air outside of the boundary layer.**

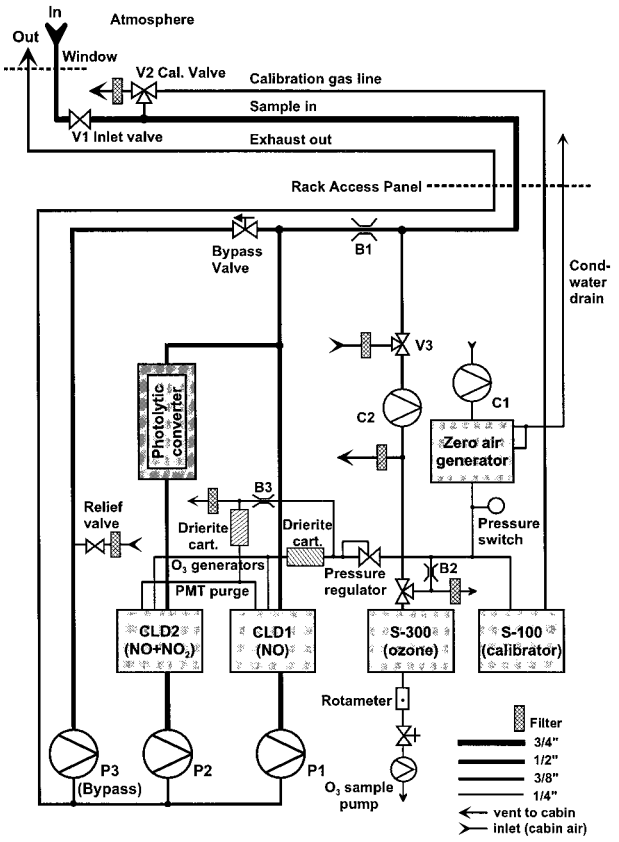


**FIGURE 3. System flow diagram. Abbreviations as in Figure 1 except B1, B2, B3, indicate the flow restrictors (critical orifices) and V3 indicates the O3 analyzer test valve. The pressure switch monitors the functioning of the zero air generator. B2 and B3 supply controlled flows of zero air to the $O_3$ analyzer and the PMT purge line in the $NO_x$ analyzers. The Drierite cartridges in the latter supply ensure that the dew point of the purge air remains well below the PMT temperature. The pressure regulator ensures a constant flow of zero air to the $O_3$ generators in the CLD instruments independent of cabin pressure.**

(P1 in Figures 1 and 3). This is a rotary-vane type (Leybold AG, Germany, type TRIVAC S16B) using perfluorinated polyether fluid (Fomblin Y L-VAC 14/6, manufactured by Montefluos, Milan, Italy) as the operating medium to provide the pump with the highest possible resistance to attack by ozone. This was necessary to protect the pump in case the ozone scrubber failed during measurement. An oil recirculating filter (OF) removes any oil mist from the exhaust flow and returns this to the pump.

**$NO_2$ Analyzer.** The $NO_2$ analyzer (CLD2 in Figures 1 and 3) consisted of an CLD 780 TR instrument, as described above, in conjunction with an ECO PHYSICS PLC 762 photolytic converter in which the sample gas is irradiated by the collimated beam of a 1000 W xenon discharge lamp. This causes the photolytic decomposition of $NO_2$ into NO with the production of $O_3$ (*21*):

$$NO_2 + h\nu \rightarrow NO + O$$

$$O + O_2 + M \rightarrow O_3 + M$$

where M represents a neutral collision partner.

To reduce effects from other potential intereferents (e.g., $HNO_3$), the lamp output is spectrally filtered to remove all but the 320−400 nm wavelength range and the optical system is arranged to minimize wall effects. The glass photolysis cell is cooled to a temperature between 5 and 10 °C by means of three rows of Peltier elements to reduce the probability of interference due to the thermal dissociation of peroxyacetyl nitrate (PAN), $HNO_4$, and $N_2O_5$ in the sample air (*22*). The lamp power supply and cable were modified to reduce the electromagnetic interference caused by the 30 kV, microsecond-duration ignition pulse (this factor being of course critically important in an aircraft environment). The conversion efficiency achieved by the photolysis cell at the stabilized operating pressure of 85 hPa and sample flow rate of 3 L/min (STP) is typically 65% during flights. This was measured regularly in-flight during each calibration procedure, the required $NO_2$ being generated by the gas-phase titration of calibration-concentration NO with $O_3$ generated within the calibrator unit. A useful feature of this procedure was that a reduction of the conversion efficiency invariably heralded the imminent demise of the Xe lamp. Lamp lifetime was generally about 1000 h, as specified by the manufacturer. The dimensions of the cell (800 mm long by 50 mm i.d.) give a residence time of 2.6 s (assuming plug flow) and a 0−95% rise time of approximately 3 s.

**$O_3$ Analyzer.** The $O_3$ analyzer was a modified Environics, Inc. (U.S.A.) S-300 instrument which uses the well-known method of measuring the UV absorption of ozone in the sample at 253.7 nm. To improve sensitivity, the absorption tube length was increased from 30 to 75 cm and the ambient air (typically at 200 hPa) was compressed to aircraft cabin pressure (about 800 hPa) using a poly(tetrafluoroethylene) (PTFE)-coated diaphragm pump (Vacuubrand GmbH, Germany, type MZ2C - C2 in Figures 1 and 3). To increase the speed of response the flow rate was increased from 2 to 4.5 L/min (STP). Instead of using the standard technique of switching the sample flow through an ozone scrubber to create "reference" air for the instrumental zero signal, externally generated zero air was used to preclude the possibility of the scrubber slowly becoming saturated and falsifying the measurement. Other electronic and mechanical alterations were made to the instrument to enhance its robustness. The modified instrument was capable of detecting 500 pptv in 4 s with a 0−95% rise time of 2 s.

Typically NO and $NO_2$ values are obtained every 3 s, and an $O_3$ value every 4 s. This corresponds to a spatial separation of about 700 to 1000 m between samples. Details of the performance of the NO, $NO_2$, and $O_3$ measuring instruments are given later in the Quality of $O_3$, NO, and $NO_2$ Measurements section.

**Sampling System.** Figure 3 is the system gas flow diagram, showing the sample flow, inlet pressure stabilization system, zero air supply, and calibration gas path. The air sample is obtained through an aerofoil-sectioned aluminum boom with a PTFE core, mounted on an aluminum plate which replaces the second window just forward of the aircraft's rearmost starboard door. The boom extends 9 in. (approximately 23.5 cm) into the slipstream from the aircraft skin as shown in Figure 2. Air is drawn into the rearward facing 5/8 in. (15.9 mm) i.d. aperture at the tip of the boom and is then carried through the boom and to the instrumentation rack through a 5 m long sample line (3/4 in. o.d. PTFE tubing with an inner diameter of 5/8 in.).

The sample pressure at the inlet to the NO and $NO_2$ analyzers is held constant at 85 hPa by the use of a critical orifice and bypass system in which air in excess of that required by the instruments is pumped away, through a motor-driven needle valve, by a third vacuum pump of the same type as used for the NO and $NO_2$ analyzers (P3 in Figures 1 and 3). The bypass system also ensures a constant residence time of the air in the sample line irrespective of the ambient air pressure. The relatively large sample flow rate of 12 L/min (STP) at 200 hPa ambient pressure keeps the residence time at 0.9 s.

A PTFE solenoid valve (Figure 3 V1) located near the sample line inlet is opened after takeoff and closed before landing to avoid contamination of the sample line on the ground. In addition, the sample line is reverse-flushed with zero air during the warm up and shutdown phases. A second PTFE solenoid valve (V2) is used to switch between sample and calibration gas. Calibration gas enters the sampling path as close to the boom as possible to account for possible heterogeneous losses in the long sampling line.

**Calibration System and Zero Air Supply.** Calibration gas (6 ppmv NO in $N_2$, supplied by Carbagas, Switzerland) is stored in a 1 L cylinder filled to only 50 bar for safety reasons (the normal cylinder filling pressure being 200 bar). A concentration of 20 ppbv NO was used for the analyzer sensitivity calibration and photolytic converter efficiency measurement, so calibration gas was diluted with air from the zero air generator (ECO PHYSICS type PAG 002, supplied with compressed cabin air from compressor C1). The dilution ratio is maintained by a multigas calibrator (Environics Inc., model S100) which also generated the ozone used in the photolytic converter efficiency measurement. Zero air is also used to calibrate the instrument zero points and as zero reference gas for the ozone analyzer. In addition, the ozone generators and PMT purge circuits in the NO and $NO_2$ instruments are also supplied with zero air, the former via a pressure regulator (to compensate for the fact that the cabin pressure varies with aircraft altitude between about 800 and 1000 hPa) and the latter at cabin pressure via a flow restrictor (B3 in Figure 3). No variation in the calibrator dilution ratio was observed with varying cabin pressure. Either the mass flow controllers used were not susceptible to this effect (no information on this point could be obtained from the manufacturer) or possibly both devices had similar pressure characteristics and thus maintained a constant dilution factor.

**Control and Data Acquisition System.** System control is maintained by a computer which is also interfaced to the aircraft data buses—the digital flight data recorder (DFDR) bus (via a test output on the crash recorder unit) and the Airshow-System, which provides positional data for the visual presentation of a few selected flight parameters to passengers during the flight. The interface, designed and built by the staff of the Neutechnikum Buchs in Switzerland, filters a selected set of meteorological (temperature, pressure, horizontal wind), positional (latitude, longitude), and aircraft system information from the data buses which is required for the automatic start up and shutdown of the NOXAR system just after takeoff and before landing, respectively. The aircraft data is stored at a rate of 1 set/s, together with the data from the analyzers, on shock and vibration resistant PCMCIA hard disks (Intégral Peripherals, U.S.A.) which were exchanged about once a week. Because of restrictions imposed by the pilots' labor union, the recording of aircraft data was only allowed at altitudes above 10 000 ft (asl). Many diagnostic parameters—instrument pressures and temperatures, error status information, and digital output signals from several components flagging operations such as valve-switching or power ups—were stored at regular intervals for postflight inspection and retrieval. This diagnostic information proved invaluable when system- or instrument-based problems were encountered and also for routine monitoring of system operation.

**Electrical and Electronic System.** Power is drawn from the standard aircraft three-phase galley supply at 115 VAC 400 Hz, 3 × 20A (6.5 kW). To eliminate cable-borne EMI effects in both directions, the power receptacle actually extends into the housing of a 4 × 25A high-performance line filter (Schaffner Elektronik AG, Switzerland, type FN 354-25/03) mounted on the lower side of the rack top panel. The filtered 115 VAC supply is fed to the control computer, watchdog, and emergency shutdown circuits, and also (via a three-phase relay) to two paralleled 3.5 kW frequency converters (Avionic Instruments Inc., U.S.A., type 4B3500) which provided the single phase 230 VAC 50 Hz for the main system. This was used by all units except the $NO/NO_2$ analyzers and the photolytic converter (excluding the PLC lamp power). These devices were supplied by a 28 VDC 900W power supply (Astec America Inc., U.S.A., type VS1-C6-00) which was in turn powered from the 230 VAC 50 Hz system.

**Mechanical Design and Safety Features.** The rack was manufactured by Bucher Leichtbau AG, Switzerland, to meet the static load requirement stipulated by Swissair and the Swiss Federal Civil Aviation Authority (FOCA) of 3G in all directions, a further condition being the containment of the rack contents up to 9G. A structural analysis was performed by SL Designs, Southampton, U.K., to ensure that it would meet these requirements.

Air flow through the rack is provided by two fans mounted on the sides of the rack, operating in push−pull mode, thus ensuring that the critical instruments are always adequately cooled with fresh air. The individual capacity of each one of the 110 W fans (2100 $m^3$/h in free air) is sufficient to ensure that the rack will not overheat even if the other should malfunction. The rack itself (and indeed the freight compartment in general) is monitored from the cockpit by an IR video camera.

Active safety features included a three-level fire prevention scheme. The detection of a temperature in excess of 50 °C by one of three electronic sensors distributed through the rack causes a controlled shutdown of the NOXAR system to the standby mode, but does not otherwise generate an alarm. Should the internal temperature reach 60 °C, then one of the second-level safety devices—three bimetallic thermostats—operates, causing the immediate total shutdown of the system. Furthermore, an audible alarm is then generated in the rear galley which can only be interrupted by the cabin crew operating a switch. The system can now only be restarted by a manual reset from within the rack. The third level of fire defense is provided by six compact extinguishers placed in each compartment which automatically fill the rack with Halon vapor when the temperature exceeds 73 °C. Of note in this context is the fail-safe operation of the ventilation shutters, which are designed to close on power down, thus containing any fire (and extinguishing medium) within the rack.

To ensure in advance that the system would—as required by Swissair—have no significant effect on flight operations, the complete rack successfully underwent electrical tests for conducted and radiated interference (as per the Radio Technical Commission for Aeronautics document RTCA/DO-160B, "Environmental Conditions and Test Procedures for Airborne Equipment", Section 21 Emission of Radio Frequency Energy, Category Z) at a FOCA-certified testing facility (Oerlikon-Contraves AG, EMC-Test Centre Zürich). Despite this certification, acceptance by Swissair was still conditional on comprehensive electrical tests being made after the rack was installed in the aircraft to ensure that it had no effect on the aircraft systems. No problems were encountered at this critical phase, and the system was accepted by Swissair for a 1 year operation period beginning May 1995 without further tests being necessary.

The dimensions of the rack are (maximum width × depth × height) 3 × 1 × 1.2 m, with a total weight of 580 kg.

## System Operation and Performance

From May 1995 to May 1996, the aircraft logged some 540 flights, mainly along three routes—North Atlantic (Zurich—New York, Atlanta, Boston, Chicago; 269 flights), Far East South (Zurich—Bombay, Hong Kong; 145 flights) and Far East North (Zurich—Beijing, Shanghai; 129 flights). This gave about 4000 h of data, corresponding to partial or full system in-service time of around 80%.

**Mode of Operation.** The two chemiluminescence analyzers are operated in a similar way as described in ref *23*, and details are given in the Ph.D. thesis by D. Brunner (*24*). Photon counts are integrated over 3 s time intervals which are synchronized with the aircraft data system. Computer-controlled zero calibrations using air from the zero air generator are performed every 20 min which allows the drift of the instrumental zero signal to be determined. Fluctuations of this signal on shorter time scales add to the measurement noise. Every 3 h, and thus typically twice per flight, a full calibration cycle including a zero calibration, a sensitivity calibration, and a photolytic converter efficiency measurement are performed. Linear interpolations are made between calibrations to derive the appropriate values for each measurement. The $NO_2$ concentration is calculated by taking the difference between the NO concentrations measured by the two analyzers and dividing this by the efficiency of the photolytic converter. The effect of the reverse reaction of NO with both atmospheric ozone and that generated by the photolysis reaction is also accounted for (*21*, *24*). The NO channel signal is smoothed using a numerical filter calculated from the experimentally determined response function of the photolytic converter to ensure that the NO and $NO_2$ analyzers' signals are synchronized and directly comparable.

$O_3$ samples are obtained at roughly 4 s intervals. Unfortunately, the internal software does not allow synchronization of the instrument with the other measurements. In theory, no calibration of the $O_3$ analyzer is required because the only difference in the sample and reference measurements is due to absorption by ozone under known conditions (the absorption path length and ozone absorption coefficient are both known accurately). However, to ensure its proper operation, functional checks are made every 3 h, as part of the full calibration cycle, by supplying a roughly known quantity of $O_3$ to the instrument and monitoring the measurement values for plausibility.

**Potential Contamination Sources.** The position of the sampling inlet near the tail of the aircraft required detailed consideration of the possibility that the sampled air might be contaminated by engine exhaust gas. Furthermore, because safety and cost considerations precluded the use of a sample probe extending out of the boundary layer of the aircraft (see Figure 2), possible heterogeneous losses on the aircraft skin had to be considered. Worst-case calculations based on aerodynamic data provided by Boeing engineers indicated that the average number of collisions each molecule underwent with the fuselage before being sampled was less than a hundred. This number was compared with sticking coefficients of $O_3$ and $NO_2$ on different surfaces (*25*, *26*) which are expected to be more reactive than the painted aircraft skin (the paint is a modified polyurethane lacquer with inert titanium oxide pigments) for which adequate information was not available in the literature. Realistic sticking coefficients of $O_3$ and $NO_2$ are probably below $10^{-4}$, which gives a maximum loss of 1% of $O_3$ and $NO_2$. The excellent agreement between the NOXAR $O_3$ data and simultaneous measurements of the MOZAIC program over the North Atlantic (described later) demonstrates that $O_3$ losses on the aircraft skin were not a significant problem. The possibility of sampling exhaust air from the engines of the B-747 was ruled out by Boeing engineers, and this was confirmed by actual NO concentrations measured during the campaign, which always showed the expected near-zero value during night flights (see Figure 5).

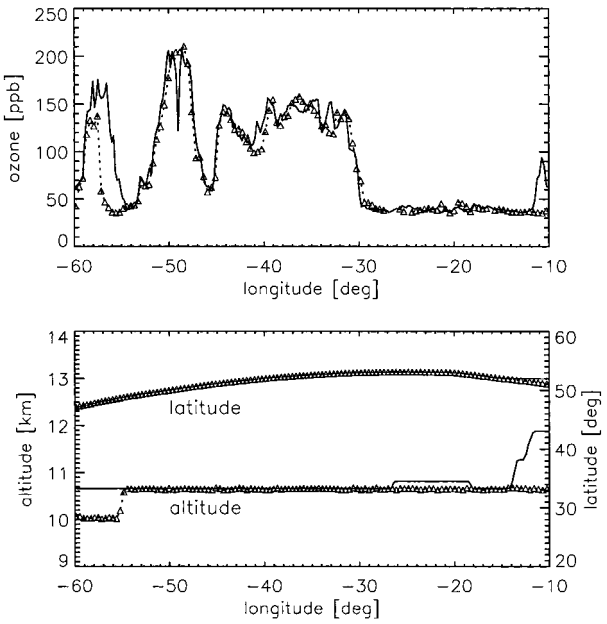


**FIGURE 4. Comparison of the measurements from the NOXAR B-747 and a MOZAIC Airbus A-340 aircraft on "simultaneous" flights from Dec 20, 1995, over the North Atlantic. Time difference between the two observations is 30 min. Solid lines: MOZAIC (1 min avg). Dashed lines with △ symbols: NOXAR (2 min avg).**

**Quality of $O_3$, NO, and $NO_2$ Measurements.** The experimentally determined contributions to the precision and accuracy of each instrument and the overall uncertainties, taken as the sum of the precision and accuracy, are summarized in Table 1. Errors are listed for 2 min averaged data if not stated otherwise.

The ozone analyzer was calibrated before and after the campaign against a U.S. EPA (Environmental Protection Agency) traceable reference standard instrument owned by ECO PHYSICS in order to determine possible ozone losses in the sampling lines. Significant losses were only found after the campaign, and these were mainly attributable to the PTFE-coated compressor upstream of the analyzer whose surface properties probably slowly degraded during the 1 year measuring period. (With hindsight, we recommend that when using such a compressor it should be cleaned and serviced more frequently, perhaps quarterly). The losses were corrected for by assuming a linear increase of the effect with

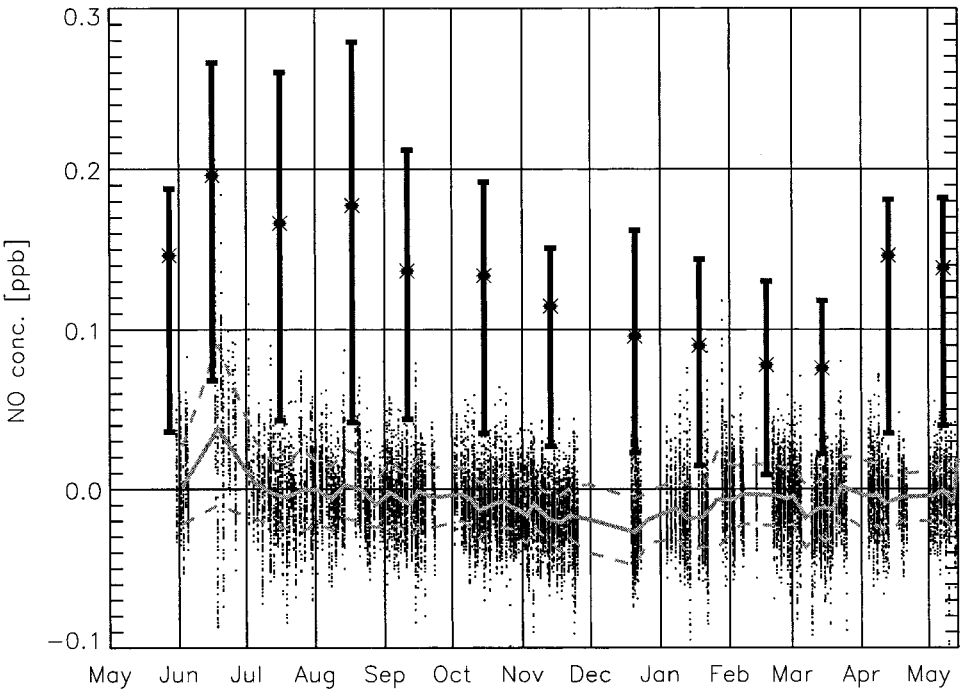


**FIGURE 5. Day- and nighttime NO measurements. The points represent all nighttime NO measurements (2 min integrated values) during the NOXAR campaign between May 1995 and May 1996. The gray solid line is a 500 point average through these points. The dashed lines connect the standard deviations ($\pm 1\sigma$) of each 500 point bin. The vertical bars denote the central 67% (i.e., the range between the 17% and 83% percentiles) of all offset-corrected daytime NO measurements in each month. Crosses are monthly mean daytime NO concentrations.**

**TABLE 1. Experimentally Determined Uncertainties in the 2 min Averaged $O_3$, NO, and $NO_2$ Measurements**

| | type of error | source of uncertainty | uncertainty |
|---|---|---|---|
| $O_3$ | precision | in-flight and on-ground tests (4 s avg) | 0.3−0.5 ppbv |
| | accuracy | reference standard instrument | ±1% |
| | | calibration against standard instrument | ±1.5% |
| | | ozone losses in sampling line | ±3.5% |
| | | zero (or reference) air offset | ±5 ppbv |
| | | total accuracy | ±5 ppbv ± 6% |
| NO | precision | standard error in nighttime NO | ±19 pptv |
| | accuracy | instrumental artifact (nighttime offset) | ±4.3 pptv |
| | | NO content in calibration gas cylinders | ±2.8% |
| | | linear decrease in NO content | ±2% |
| | | precision of in-flight sensitivity calibrations | ±3.5% |
| | | total accuracy | ±4.3 pptv ± 8% |
| $NO_2$ | precision | error in $NO_C$ measurement ($NO_C$ = NO + converted $NO_2$) | ∼same as for NO |
| | | corresponding error in $NO_2$ | ±41 pptv |
| | accuracy | instrumental artifact | ±4.3 pptv |
| | | NO content in gas cylinders + error in mass flow controller (same as for NO) | ±5.8% |
| | | sensitivity calibrations of both instruments | ±4% |
| | | precision in conversion efficiency calibration | ±0.5% |
| | | $NO_2$ content in calibration gas cylinder | ±1% |
| | | total accuracy | ±4.3 pptv ± 11% |
| | | interferences | ≈+33 pptv ? |

operating time. The uncertainty in the $O_3$ measurement associated with these losses is estimated to ±50% of the maximum loss of 7%. Another problem was caused by the use of a zero air generator instead of an ozone scrubber to produce reference air. A differing humidity of the sample and reference air was found to generate an offset in the $O_3$ measurement—most probably due to small changes in the optical properties of the absorption cell, a long tube which acts somewhat like a waveguide for the light from the UV lamp. The associated uncertainty was estimated to ±5 ppbv for air samples at ambient air temperatures below −40 °C by comparing the signal offset produced by different zero air types with dew points between −60 and −20 °C. Figure 4 shows a comparison of the $O_3$ measurements on a North Atlantic flight from December 20, 1995, with "simultaneous" measurements from a MOZAIC Airbus A340 (*19*). A linear fit through a scatter plot of the closest NOXAR and MOZAIC $O_3$ measurements (270 2 min samples at the same flight level, horizontal distance < 40 km, time difference < 1 h) on this and a few other flights shows an excellent agreement for the observed range of concentrations between 40 and 400 ppbv at cruise altitude. The linear fit is

$$[\text{MOZAIC-O}_3] = 1.5\ \text{ppbv}\ (\pm 1.5\ \text{ppbv}) + 0.997\ (\pm 0.014)\ [\text{NOXAR-O}_3] \quad (1)$$

The precision of the NO measurement was estimated conservatively by calculating the standard deviation of all nighttime measurements about the mean. The mean was expected to be zero since NO is rapidly titrated by atmo-

spheric $O_3$ at night. However, a small offset was usually present as shown in Figure 5, which was believed to be caused by an instrumental artifact. A time-dependent offset correction was therefore applied to all measurements, assuming that the same artifact was present during day and night. The correction averaged 8 pptv and was largest in June, when the analyzer was replaced for 10 days by an identical instrument which showed a much higher noise level and produced a larger artifact signal. Except for this 10 day period, the noise level of the NO measurement remained very stable at about 20 pptv during the campaign, as indicated by the dashed lines in Figure 5. The daytime NO concentrations were usually well above the detection limit except during winter when NO concentrations often dropped below 20 pptv. The sensitivity of the detector was calibrated typically twice per flight and was very stable within 15% during the whole campaign. This stability was ensured by cross-calibrating each calibration gas cylinder against one single reference cylinder.

The accuracy of the NO measurement is thus mainly determined by errors in the correction of the instrumental artifact and by errors in the sensitivity calibrations due to uncertainties in the calibration gas cylinder content and the mass flow controllers used to dilute the calibration gas.

The $NO_2$ measurement suffered both from contamination problems and the high detection limit which usually exceeded the low concentrations observed during the day. Within a few months of the system being commissioned, it became apparent that there was some effect which caused the analyzer counts to increase greatly when the photolysis lamp was switched on with zero air sample. This effect was 1 order of magnitude smaller in a benchtop photolysis converter of the same type used as a comparison and was degrading the quality of the $NO_2$ data, so the flight unit was replaced in November 1995. Inspection of the cell revealed severe particulate contamination. After the cell was thoroughly cleaned, it was replaced in the converter, following which the anomalous count increase disappeared. The contamination was probably caused by the system having, for some reason, automatically started up on the ground, possibly during maintenance work on the aircraft during which signals simulating flight conditions were transmitted on the data bus without our knowledge. After this experience, given the evident sensitivity of the technique to contamination, the photolysis tube was regularly inspected. $NO_2$ measurements before November 1995 could therefore only be used qualitatively.

The uncertainty in the $NO_2$ measurement was determined in a way similar to that for the NO analyzer (see Table 1). The overall uncertainty is much larger since the $NO_2$ concentration is given by the difference of two individual measurements divided by a conversion efficiency of about 0.65. Additionally, the artifact signal of this instrument could not be corrected in the same way as that for the NO channel.

Because of the problems encountered with the $NO_2$ measurement, theoretical $NO_2$ concentrations were calculated from measured NO and $O_3$ concentrations which gave $NO_x$ values for the whole measuring period. This calculation assumes a simple photostationary equilibrium between $NO_2$, NO, and $O_3$. The $NO_2$ concentration is then given by

$$[NO_2] = k_1[NO][O_3]/J_{NO2} \quad (2)$$

where $k_1$ is the reaction rate constant of the reaction of $O_3$ with NO and $J_{NO2}$ is the $NO_2$ photolysis rate. Photolysis rates were calculated for clear-sky conditions from all daytime NO and $O_3$ measurements at solar zenith angles $<85°$ using the STAR (system for transfer of atmospheric radiation) model (*27*). The relatively large uncertainty in the calculation of $NO_2$, which assumes clear-sky conditions and neglects the presence of peroxy radicals which may change the simple equilibrium (*2*), adds to the uncertainty in total $NO_x$ by not more than 20% because $NO_2$ is usually only a minor fraction of total $NO_x$. $NO_x$ concentrations derived from measured $NO_2$ concentrations were 33 pptv higher on average than $NO_x$ concentrations calculated from photostationary state $NO_2$. Given the annual average $NO_x$ concentration of 172 pptv, this represents a difference of 20%.

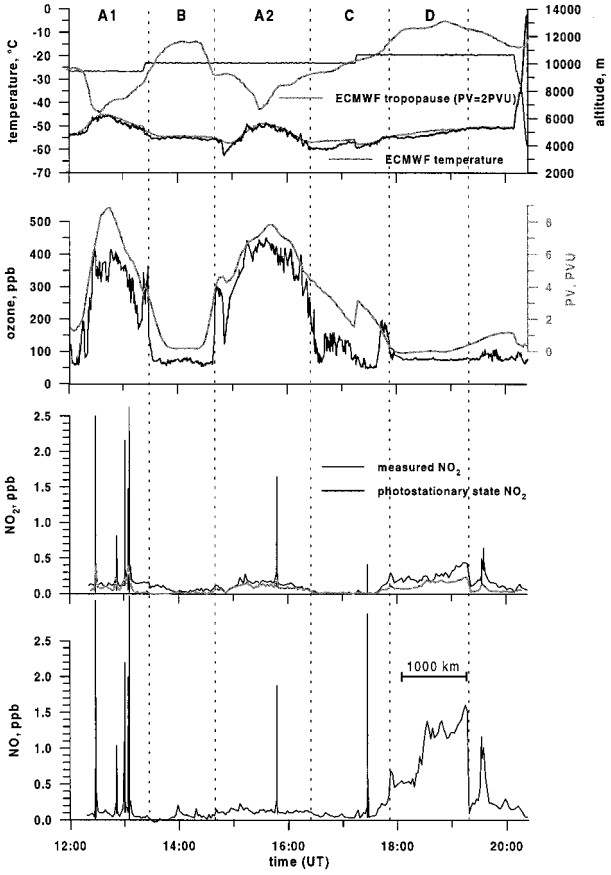


**FIGURE 6. Time series plot of a flight from Zurich to Atlanta from May 10, 1996. See text for details.**

The linear fit between all measured $NO_2$ and photostationary state $NO_2$ values from December 1995 until May 1996 is

$$[NO_2]_{meas} = 36 \text{ pptv } (\pm 0.6 \text{ pptv}) + 0.946\ (\pm 0.0087)\ [NO_2]_{calc}\ (r = 0.73) \quad (3)$$

The intercept is significantly ($P = 0.0001$) different from zero, indicating that there was either an instrumental problem or the measurements suffered from interferences, e.g., due to thermal and wall-catalyzed decomposition of $N_2O_5$ and $HNO_4$ in the sampling lines and the photolytic converter.

## Discussion of Typical Features Observed in the Measurements

Here we demonstrate some of the most typical and important $NO_x$ and $O_3$ features observed during the 1 year measurement campaign based on data from a single exemplary flight. Figure 6 shows the time series of various parameters measured on the flight from Zurich to Atlanta on May 10, 1996. The $NO_x$ data are presented as 2 min averages in order to reduce the statistical noise which is evident in the 3 s samples. In the vicinity of sharp peaks, the $NO_x$ data are plotted with 3 s resolution because the 2 min averages would hide these short-time features. The other parameters are shown as 3 s

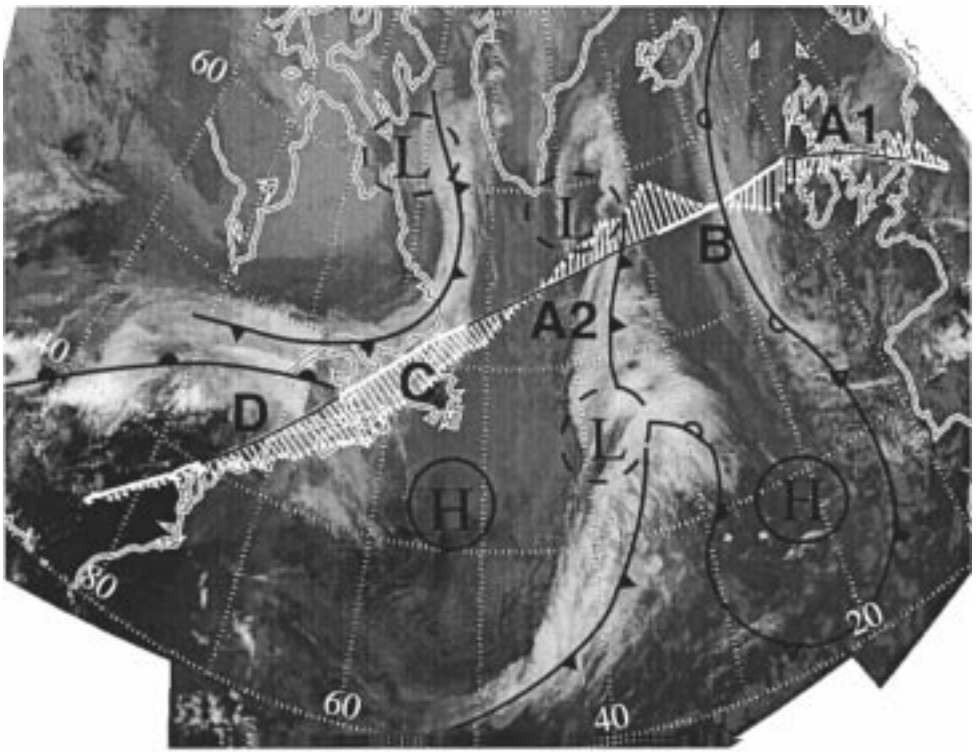


**FIGURE 7. Flight track and wind vectors measured from the B-747 plotted over a series of four NOAA AVHRR channel 4 satellite images of the same day. Start times of image creation (from right to left): 12:28 UTC, 14:07 UTC, 17:20 UTC, and 19:03 UTC. Note that the cloud pattern and the surface lows, highs, and fronts mainly represent features at low altitudes.**

averages. Potential vorticity and temperature from the European Centre for Medium-Range Weather Forecasts (ECMWF) analysis (version T213/L31) were interpolated in time and space to the flight track of the B-747. The altitude of the tropopause, which is taken as a surface of constant potential vorticity (PV = 2 PVU), is shown in the top panel together with the flight altitude.

Figure 7 shows the flight track of the aircraft and measured wind vectors plotted over a series of four infrared satellite images from NOAA polar orbiting satellites to illustrate the different meteorological conditions encountered during the flight. The sequence of satellite images roughly follows the aircraft on its 9 h flight starting in Zurich at 11:35 a.m. (UTC). Different flight sections referred to later in the text are marked in the figure by capital letters. The positions of some low-level features closely related to the cloud pattern on the satellite images are also shown in the figure. The analysis of these surface lows, highs, and fronts was adopted from "Berliner" and "DWD" (Deutscher Wetterdienst) weather charts.

As the B-747 loses weight through fuel combustion, it ascends stepwise from an initial flight level of 9.5 km to 10.8 km just before its descent into the destination airport Atlanta. The air temperature at cruise altitudes close to the tropopause varies between −45 and −60 °C. Airmasses encountered in flight sections A1 and A2 are characterized by high values of potential vorticity (>2 PVU) and by ozone concentrations of up to 450 ppbv and are clearly of stratospheric origin. They are distinctly separated from section B where the ozone abundance is of the order of 70 ppbv, a typical value for air originating in the upper troposphere. Region A2 corresponds to an upper level trough possibly associated with the two cyclones in Figure 7 at about 38° W. The wind direction changes from generally northerly upstream of the trough (i.e., to the west) to southerly at the outflow (i.e., to the east). The center of the trough is marked by minimal wind speed and a 180° change of wind direction. As a consequence of the southward expansion of the trough during the previous days, polar air has been transported into region A2 along isentropic surfaces sloping downward from north to south. In this way, ozone-rich air originating in the lower polar stratosphere has been carried to and below aircraft cruising altitudes. Region A1 marks a second trough over Great Britain with similarly high ozone concentrations. Low ozone levels are found in airmass B which is characterized by moist air (humidity derived from ECMWF analysis is not shown) originating in the troposphere southward of the polar jet stream. At low levels the polar air in region A2 and the warmer air in region B are separated by a cold front which is clearly visible in the satellite images as a band of compact clouds extending from southeast of Greenland down to 30°N latitude. The cold front extends up to the aircraft flight altitude causing a sharp temperature drop of 8 °C as seen in the top graph in Figure 6. Due to the low horizontal resolution of the ECMWF temperature data, the frontal structure is not properly resolved. At the same time, ozone drops from 300 ppbv ahead of the front to 120 ppbv just behind it. This demonstrates that convective activity along cold fronts may inject tropospheric air into the lowest levels of the stratosphere and may therefore modify the chemical composition of the lowermost stratosphere.

The $NO_x$ concentration in the trough regions A1 and A2 is distinctly higher than that just outside. Except for the winter flights, this behavior was very often observed and supports the common belief that transport of $NO_x$ from the stratosphere where it is formed by the decomposition of $N_2O$ is a source of upper tropospheric $NO_x$ (*28*). Striking features in Figure 6 are the numerous short-time $NO_x$ peaks which are most probably due to sampling exhaust plumes from other aircraft in the flight corridor. Similar observations have been recently described in ref *29*, where, based on radar observations, the authors were able to identify the source aircraft of plumes having peak concentrations of up to 2.5 ppbv. The major aircraft exhaust signatures were due to relatively fresh emissions, i.e., superpositions of 2−5 plumes with ages between 15 min and 3 h. During the NOXAR

measurement period, 2800 peaks of typically 1−10 ppbv and lasting 3 to 30 s were identified. Flight section D marks a region extending several hundred kilometers along the flight track where high $NO_x$ concentrations of up to 2 ppbv were observed. Such broad $NO_x$ plumes were detected on many flights (several hundred cases were identified) although usually less pronounced than in this case. These features are believed to be caused by rapid vertical transport of polluted air from the planetary boundary layer and/or by lightning activity in convective clouds followed by large scale dispersion at tropopause altitudes. To the west of flight section D, the remainder of a convective cloud cluster is visible. The brightness temperature of the brightest pixels in the NOAA satellite image over this region is between −68 and −63 °C. Although the real temperatures of the cloud tops might have been somewhat higher if the emissivity of the clouds was below unity, the cold temperatures suggest that the highest clouds were extending up to the tropopause. Strong updrafts in these heavy thunderstorm clouds may have transported moist air from the boundary layer to the upper troposphere where the air has been fanned out to the U.S. east coast and further out over the Atlantic by the strong winds observed from the B-747 over this region. The moist air is probably responsible for the band of cirrus clouds extending from the cold front to the north of the flight track toward the anticyclone southeast of section D. The low and even negative values of potential vorticity in section D provide further evidence that this airmass was influenced by convective processes (*30*). Unfortunately, the limited information about its chemical composition does not allow its unambiguous identification as boundary layer air. Moreover, the source of the high $NO_x$ levels in the upper troposphere—whether produced by lightning activity or on the ground—cannot be definitely established since both are linked to deep convection.

## Summary

The NOXAR experiment provides the first climatological data set on $NO_x$ and ozone concentrations in the tropopause region over large parts of the northern hemisphere. The measuring system in general performed well, with an acceptable level of operational problems despite the harsh environment in which it had to operate. The NO and $O_3$ measurements were stable and reliable over the whole measuring period. The $NO_2$ measurement suffered from various problems including contamination and low precision and is therefore of much lower quality. Our belief that careful design of the system with attention focused on robustness while maintaining ease of accessibility was vindicated by the high level of operational readiness. Even so we learned several important lessons as a result of our experience with the photolytic converter and ozone sample compressor.

The data set, although yet to be fully analyzed, provides new insight in the processes that govern the distribution of nitrogen oxides and ozone in the tropopause region and will contribute to reducing the uncertainties in the $NO_x$ abundance at aircraft cruising altitudes as calculated by current chemical transport models.

Update: The NOXAR instrumentation packet was again operated for three months in autumn 1997 under the European POLINAT II program.

## Acknowledgments

The NOXAR project was funded by the Swiss Federal Office for Civil Aviation (FOCA), Bern, Switzerland. We furthermore acknowledge the generous support by Swissair in bearing the costs of carrying of the instrumentation, the excellent cooperation and support of F. Stössel, B. Sterchi, and H-P. Roth (Swissair), L. Vonlanthen, F. Blauenstein, and W. Bula (FOCA), and the advice of H. Richner (Atmospheric Science, ETH-Z). We are indebted to A. Marenco, the coordinator of the MOZAIC program, for providing us access to the MOZAIC database. ECO PHYSICS AG thanks all the numerous suppliers whose cooperation contributed significantly to the success of the NOXAR project.

## Literature Cited

(1) Finlayson-Pitts, B.; Pitts, J. N., Jr. *Atmospheric Chemistry*; John Wiley and Sons: New York, 1986.
(2) Lippmann, M. *Environ. Sci. Technol.* **1991**, *25*, 1954−1962.
(3) Prinz, B. *Proceedings of the NATO Advanced Workshop on Regional and Global Ozone Interaction and its Environmental Consequences, Lillehammer, Norway, June 1−5, 1988*; D. Reidel Publishing: Dordrecht, Holland, 1988.
(4) Roelofs, G. J.; Lelieveld, J.; van Dorland, R. *J. Geophys. Res.* **1997**, *102*, 23389−23401.
(5) Lacis, A. A.; Wuebbles, D. J.; Logan, J. A. *J. Geophys. Res.* **1990**, *95*, 9971−9981.
(6) Brasseur, G. P.; Müller, J. F.; Granier, C. *J. Geophys. Res.* **1996**, *101*, 1423−1428.
(7) Schumann, U. *Ann. Geophys.* **1994**, *12*, 365−384.
(8) *Scientific Assessment of Ozone Depletion: 1994*. Global Ozone Research and Monitoring Project−Report No. 37. World Meteorological Organization: Geneva, 1995.
(9) Stolarski, R. S.; et al. *1995 Scientific Assessment of the atmospheric effects of stratospheric aircraft*; NASA Ref. Publication 1381, Washington, DC, 1995.
(10) *Atmospheric Effects of Subsonic Aircraft: Interim Assessment Report of the Advanced Subsonic Technology Program*; Friedl, R. R., Ed.; NASA Ref. Publication 1400, Greenbelt, MD, 1997.
(11) Schumann, U. *Atmos. Environ.* **1997**, *31*, 1723−1733.
(12) Beck, J. P.; Reeves, C. E.; De Leeuw, F. A. A. M.; Penkett, S. A. *Atmos. Environ.* **1992**, *26A*, 17−29.
(13) Kraus, A. B.; Rohrer, F.; Grobler, E. S.; Ehhalt, D. H. *J. Geophys. Res.* **1996**, *101*, 18587−18604.
(14) Flatøy, F.; Hov, Ø. *J. Geophys. Res.* **1996**, *101*, 1401−1422.
(15) Lee, D. S.; Köhler, I.; Grobler, E.; Rohrer, F.; Sausen, R.; Gallardo-Klenner, L.; Olivier, J. G. J.; Dentener, F. J.; Bouwman, A. F. *Atmos. Environ.* **1997**, *31*, 1723−1733.
(16) Emmons, L. K.; et al. *Atmos. Environ.* **1997**, *31*, 1851−1904.
(17) *Pollution from Aircraft Emissions in the North Atlantic Flight Corridor (POLINAT)*; Schumann, U., Ed.; Air Pollution Research Report 58 (EUR 16978 EN); Office for Official Publication of the European Communities: Luxembourg, 1996.
(18) Nastrom, G. D. *J. Geophys. Res.* **1979**, *84*, 3683−3688.
(19) Marenco, A.; Thouret, V.; Nedelec, P.; Smit, H. G.; Helten, M.; Kley, D.; Karcher, F.; Simon, P.; Law, K.; Pyle, J.; Poschmann, G.; Von Wrede, R.; Hume C.; Cook, T. Submitted to *J. Geophys. Res.*
(20) Drummond, J. W.; Volz, A.; Ehhalt, D. H. *J. Atmos. Chem.* **1985**, *2*, 287−306.
(21) Kley, D.; McFarland, M. *Atmos. Technol.* **1980**, *12*, 63−69.
(22) Carroll, M. A.; Ridley, B. A.; Montzka, D. D.; Hubler, G.; Walega, J. G.; Norton, R. B.; Huebert, B. J.; Grahek, F. E. *J. Geophys. Res.* **1992**, *97*, 10361−10374.
(23) Ridley, B. A.; Carroll, M. A.; Gregory, G. L. *J. Geophys. Res.* **1987**, *92*, 2025−2047.
(24) Brunner, D. Ph.D. Thesis No. 12,556, Swiss Federal Institute of Technology (ETH), Zürich, Switzerland, 1998.
(25) Fendel, W.; Matter, D.; Burtscher, H.; Schmidtott, A. *Atmos. Environ.* **1995**, *29*, 967−973.
(26) Kalberer, M.; Tabor, K.; Ammann, M.; Parrat, Y.; Weingartner, E.; Piguet, D.; Rössler, E.; Jost, D. T.; Türler, A.; Gäggeler, H. W.; Baltensperger, U. *J. Phys. Chem.* **1996**, *100*, 15487−15493.
(27) Ruggaber, A.; Dlugi, R.; Nakajima, T. *J. Atmos. Chem.* **1994**, *18*, 171−210.
(28) Kasibhatla, P. S.; Levy, H.; Moxim, W. J.; Chameides, W. L. *J. Geophys. Res.* **1991**, *96*, 18631−18646.
(29) Schlager, H.; Konopka, P.; Schulte, P.; Schumann, U.; Ziereis, H.; Arnold, F.; Klemm, M.; Hagen, D. E.; Whitefield, P. D.; Ovarlez, J. *J. Geophys. Res.* **1997**, *102*, 10739−10750.
(30) Haynes, P. H.; McIntyre, M. E. *J. Atmos. Sci.* **1987**, *44*, 828−841.

*Received for review February 5, 1998. Revised manuscript received June 1, 1998. Accepted July 9, 1998.*

ES980119W